Search for an invisibly decaying Z' boson at Belle II in $e^+e^- \to \mu^+\mu^-(e^\pm\mu^\mp)$ plus missing energy final states

I. Adachi,[21,18] P. Ahlburg,[94] H. Aihara,[110] N. Akopov,[116] A. Aloisio,[85,33] N. Anh Ky,[30,12] D. M. Asner,[2] H. Atmacan,[96] T. Aushev,[55] V. Aushev,[77] T. Aziz,[78] V. Babu,[10] S. Baehr,[44] P. Bambade,[49] Sw. Banerjee,[99] V. Bansal,[68] M. Barrett,[21] J. Baudot,[93] J. Becker,[44] P. K. Behera,[24] J. V. Bennett,[103] E. Bernieri,[38] F. U. Bernlochner,[94] M. Bertemes,[27] M. Bessner,[97] S. Bettarini,[88,36] F. Bianchi,[90,39] D. Biswas,[99] A. Bozek,[62] M. Bračko,[101,76] P. Branchini,[38] R. A. Briere,[4] T. E. Browder,[97] A. Budano,[38] L. Burmistrov,[49] S. Bussino,[89,38] M. Campajola,[85,33] L. Cao,[94] G. Casarosa,[88,36] C. Cecchi,[87,35] D. Červenkov,[6] M.-C. Chang,[15] R. Cheaib,[95] V. Chekelian,[53] Y. Q. Chen,[106] Y.-T. Chen,[60] B. G. Cheon,[20] K. Chilikin,[50] K. Cho,[46] S. Cho,[117] S.-K. Choi,[19] S. Choudhury,[23] D. Cinabro,[114] L. Corona,[88,36] L. M. Cremaldi,[103] S. Cunliffe,[10] T. Czank,[111] F. Dattola,[10] E. De La Cruz-Burelo,[5] G. De Nardo,[85,33] M. De Nuccio,[10] G. De Pietro,[89,38] R. de Sangro,[32] M. Destefanis,[90,39] S. Dey,[80] A. De Yta-Hernandez,[5] F. Di Capua,[85,33] Z. Doležal,[6] I. Domínguez Jiménez,[84] T. V. Dong,[16] K. Dort,[43] D. Dossett,[102] S. Dubey,[97] S. Duell,[94] G. Dujany,[93] S. Eidelman,[3,64,50] M. Eliachevitch,[94] J. E. Fast,[68] T. Ferber,[10] D. Ferlewicz,[102] G. Finocchiaro,[32] S. Fiore,[37] A. Fodor,[54] F. Forti,[88,36] B. G. Fulsom,[68] E. Ganiev,[91,40] M. Garcia-Hernandez,[5] R. Garg,[69] V. Gaur,[113] A. Gaz,[57,58] A. Gellrich,[10] J. Gemmler,[44] T. Geßler,[43] R. Giordano,[85,33] A. Giri,[23] B. Gobbo,[40] R. Godang,[107] P. Goldenzweig,[44] B. Golob,[98,76] P. Gomis,[31] W. Gradl,[42] E. Graziani,[38] D. Greenwald,[79] Y. Guan,[96] C. Hadjivasiliou,[68] S. Halder,[78] T. Hara,[21,18] O. Hartbrich,[97] K. Hayasaka,[63] H. Hayashii,[59] C. Hearty,[95,29] M. T. Hedges,[97] I. Heredia de la Cruz,[5,9] M. Hernández Villanueva,[103] A. Hershenhorn,[95] T. Higuchi,[111] E. C. Hill,[95] M. Hoek,[42] C.-L. Hsu,[109] Y. Hu,[28] T. Iijima,[57,58] K. Inami,[57] G. Inguglia,[27] J. Irakkathil Jabbar,[44] A. Ishikawa,[21,18] R. Itoh,[21,18] Y. Iwasaki,[21] W. W. Jacobs,[25] D. E. Jaffe,[2] E.-J. Jang,[19] H. B. Jeon,[48] S. Jia,[1] Y. Jin,[40] C. Joo,[111] K. K. Joo,[8] J. Kahn,[44] H. Kakuno,[83] A. B. Kaliyar,[78] J. Kandra,[6] G. Karyan,[116] Y. Kato,[57,58] T. Kawasaki,[45] B. H. Kim,[73] C.-H. Kim,[20] D. Y. Kim,[75] K.-H. Kim,[117] S.-H. Kim,[20] Y. K. Kim,[117] Y. Kim,[47] T. D. Kimmel,[113] H. Kindo,[21,18] C. Kleinwort,[10] P. Kodyš,[6] S. Kohani,[97] I. Komarov,[10] S. Korpar,[101,76] N. Kovalchuk,[10] T. M. G. Kraetzschmar,[53] P. Križan,[98,76] R. Kroeger,[103] P. Krokovny,[3,64] T. Kuhr,[51] J. Kumar,[4] M. Kumar,[52] R. Kumar,[71] K. Kumara,[114] S. Kurz,[10] A. Kuzmin,[3,64] Y.-J. Kwon,[117] S. Lacaprara,[34] C. La Licata,[111] L. Lanceri,[40] J. S. Lange,[43] K. Lautenbach,[43] I.-S. Lee,[20] S. C. Lee,[48] P. Leitl,[53] D. Levit,[79] L. K. Li,[96] Y. B. Li,[70] J. Libby,[24] K. Lieret,[51] L. Li Gioi,[53] Z. Liptak,[97] Q. Y. Liu,[16] D. Liventsev,[113,21] S. Longo,[112] T. Luo,[16] Y. Maeda,[57,58] M. Maggiora,[90,39] E. Manoni,[35] S. Marcello,[90,39] C. Marinas,[31] A. Martini,[89,38] M. Masuda,[13,67] T. Matsuda,[104] K. Matsuoka,[57,58] D. Matvienko,[3,50,64] F. Meggendorfer,[53] J. C. Mei,[16] F. Meier,[11] M. Merola,[85,33] F. Metzner,[44] M. Milesi,[102] C. Miller,[112] K. Miyabayashi,[59] H. Miyake,[21,18] R. Mizuk,[50] K. Azmi,[100] G. B. Mohanty,[78] T. Moon,[73] T. Morii,[111] H.-G. Moser,[53] F. Mueller,[53] F. J. Müller,[10] Th. Muller,[44] G. Muroyama,[57] R. Mussa,[39] E. Nakano,[66] M. Nakao,[21,18] M. Nayak,[80] G. Nazaryan,[116] D. Neverov,[57] C. Niebuhr,[10] N. K. Nisar,[105] S. Nishida,[21,18] K. Nishimura,[97] M. Nishimura,[21] B. Oberhof,[32] K. Ogawa,[63] Y. Onishchuk,[77] H. Ono,[63] Y. Onuki,[110] P. Oskin,[50] H. Ozaki,[21,18] P. Pakhlov,[50,56] G. Pakhlova,[55,50] A. Paladino,[88,36] A. Panta,[103] E. Paoloni,[88,36] H. Park,[48] B. Paschen,[94] A. Passeri,[38] A. Pathak,[99] S. Paul,[79] I. Peruzzi,[32] R. Peschke,[97] R. Pestotnik,[76] M. Piccolo,[32] L. E. Piilonen,[113] V. Popov,[55,50] C. Praz,[10] E. Prencipe,[14] M. T. Prim,[44] M. V. Purohit,[65] P. Rados,[10] R. Rasheed,[93] S. Reiter,[43] M. Remnev,[3,50] P. K. Resmi,[24] I. Ripp-Baudot,[93] M. Ritter,[51] G. Rizzo,[88,36] L. B. Rizzuto,[76] S. H. Robertson,[54,29] D. Rodríguez Pérez,[84] J. M. Roney,[112,29] C. Rosenfeld,[108] A. Rostomyan,[10] N. Rout,[24] G. Russo,[85,33] D. Sahoo,[78] Y. Sakai,[21,18] S. Sandilya,[96] A. Sangal,[96] L. Santelj,[98,76] P. Sartori,[86,34] Y. Sato,[81] V. Savinov,[105] B. Scavino,[42] J. Schueler,[97] C. Schwanda,[27] R. M. Seddon,[54] Y. Seino,[63] A. Selce,[35] K. Senyo,[115] C. Sfienti,[42] C. P. Shen,[1] J.-G. Shiu,[60] B. Shwartz,[3,50] A. Sibidanov,[112] F. Simon,[53] R. J. Sobie,[112] A. Soffer,[80] A. Sokolov,[26] E. Solovieva,[50] S. Spataro,[90,39] B. Spruck,[42] M. Starič,[76] S. Stefkova,[10] R. Stroili,[86,34] J. Strube,[68] M. Sumihama,[17,67] T. Sumiyoshi,[83] D. J. Summers,[103] S. Y. Suzuki,[21,18] M. Tabata,[7] M. Takizawa,[72,22,74] U. Tamponi,[39] S. Tanaka,[21,18] K. Tanida,[41] N. Taniguchi,[21] P. Taras,[92] F. Tenchini,[10] E. Torassa,[34] K. Trabelsi,[49] T. Tsuboyama,[21,18] M. Uchida,[82] K. Unger,[44] Y. Unno,[20] S. Uno,[21,18] Y. Ushiroda,[21,18,110] S. E. Vahsen,[97] R. van Tonder,[94] G. S. Varner,[97] K. E. Varvell,[109] A. Vinokurova,[3,64] L. Vitale,[91,40] A. Vossen,[11] M. Wakai,[95] H. M. Wakeling,[54] W. Wan Abdullah,[100] C. H. Wang,[61] M.-Z. Wang,[60] A. Warburton,[54] M. Watanabe,[63] J. Webb,[102] S. Wehle,[10] C. Wessel,[94] J. Wiechczynski,[36] H. Windel,[53] E. Won,[47] B. Yabsley,[109] S. Yamada,[21] W. Yan,[106] S. B. Yang,[47] H. Ye,[10] J. H. Yin,[28] M. Yonenaga,[83] C. Z. Yuan,[28]

Y. Yusa,[63] L. Zani,[88,36] Z. Zhang,[106] V. Zhilich,[3,64] Q. D. Zhou,[21] X. Y. Zhou,[1] and V. I. Zhukova[50]
(Belle II Collaboration)

[1]*Beihang University, Beijing 100191*
[2]*Brookhaven National Laboratory, Upton, New York 11973*
[3]*Budker Institute of Nuclear Physics SB RAS, Novosibirsk 630090*
[4]*Carnegie Mellon University, Pittsburgh, Pennsylvania 15213*
[5]*Centro de Investigacion y de Estudios Avanzados del Instituto Politecnico Nacional, Mexico City 07360*
[6]*Faculty of Mathematics and Physics, Charles University, 121 16 Prague*
[7]*Chiba University, Chiba 263-8522*
[8]*Chonnam National University, Gwangju 61186*
[9]*Consejo Nacional de Ciencia y Tecnología, Mexico City 03940*
[10]*Deutsches Elektronen–Synchrotron, 22607 Hamburg*
[11]*Duke University, Durham, North Carolina 27708*
[12]*Institute of Theoretical and Applied Research (ITAR), Duy Tan University, Hanoi 100000, Vietnam*
[13]*Earthquake Research Institute, University of Tokyo, Tokyo 113-0032*
[14]*Forschungszentrum Jülich, 52425 Jülich*
[15]*Department of Physics, Fu Jen Catholic University, Taipei 24205*
[16]*Key Laboratory of Nuclear Physics and Ion-beam Application (MOE) and Institute of Modern Physics, Fudan University, Shanghai 200443*
[17]*Gifu University, Gifu 501-1193*
[18]*The Graduate University for Advanced Studies (SOKENDAI), Hayama 240-0193*
[19]*Gyeongsang National University, Jinju 52828*
[20]*Department of Physics and Institute of Natural Sciences, Hanyang University, Seoul 04763*
[21]*High Energy Accelerator Research Organization (KEK), Tsukuba 305-0801*
[22]*J-PARC Branch, KEK Theory Center, High Energy Accelerator Research Organization (KEK), Tsukuba 305-0801*
[23]*Indian Institute of Technology Hyderabad, Telangana 502285*
[24]*Indian Institute of Technology Madras, Chennai 600036*
[25]*Indiana University, Bloomington, Indiana 47408*
[26]*Institute for High Energy Physics, Protvino 142281*
[27]*Institute of High Energy Physics, Vienna 1050, Austria*
[28]*Institute of High Energy Physics, Chinese Academy of Sciences, Beijing 100049*
[29]*Institute of Particle Physics (Canada), Victoria, British Columbia V8W 2Y2*
[30]*Institute of Physics, Hanoi*
[31]*Instituto de Fisica Corpuscular, Paterna 46980*
[32]*INFN Laboratori Nazionali di Frascati, I-00044 Frascati*
[33]*INFN Sezione di Napoli, I-80126 Napoli*
[34]*INFN Sezione di Padova, I-35131 Padova*
[35]*INFN Sezione di Perugia, I-06123 Perugia*
[36]*INFN Sezione di Pisa, I-56127 Pisa*
[37]*INFN Sezione di Roma, I-00185 Roma*
[38]*INFN Sezione di Roma Tre, I-00146 Roma*
[39]*INFN Sezione di Torino, I-10125 Torino*
[40]*INFN Sezione di Trieste, I-34127 Trieste*
[41]*Advanced Science Research Center, Japan Atomic Energy Agency, Naka 319-1195*
[42]*Johannes Gutenberg-Universität Mainz, Institut für Kernphysik, D-55099 Mainz*
[43]*Justus-Liebig-Universität Gießen, 35392 Gießen*
[44]*Institut für Experimentelle Teilchenphysik, Karlsruher Institut für Technologie, 76131 Karlsruhe*
[45]*Kitasato University, Sagamihara 252-0373*
[46]*Korea Institute of Science and Technology Information, Daejeon 34141*
[47]*Korea University, Seoul 02841*
[48]*Kyungpook National University, Daegu 41566*
[49]*Laboratoire de l'Accélérateur Linéaire, IN2P3/CNRS et Université Paris-Sud 11, Centre Scientifique d'Orsay, F-91898 Orsay Cedex*
[50]*P.N. Lebedev Physical Institute of the Russian Academy of Sciences, Moscow 119991*
[51]*Ludwig Maximilians University, 80539 Munich*
[52]*Malaviya National Institute of Technology Jaipur, Jaipur 302017*
[53]*Max-Planck-Institut für Physik, 80805 München*
[54]*McGill University, Montréal, Québec, H3A 2T8*
[55]*Moscow Institute of Physics and Technology, Moscow Region 141700*
[56]*Moscow Physical Engineering Institute, Moscow 115409*
[57]*Graduate School of Science, Nagoya University, Nagoya 464-8602*
[58]*Kobayashi-Maskawa Institute, Nagoya University, Nagoya 464-8602*
[59]*Nara Women's University, Nara 630-8506*

[60]Department of Physics, National Taiwan University, Taipei 10617
[61]National United University, Miao Li 36003
[62]H. Niewodniczanski Institute of Nuclear Physics, Krakow 31-342
[63]Niigata University, Niigata 950-2181
[64]Novosibirsk State University, Novosibirsk 630090
[65]Okinawa Institute of Science and Technology, Okinawa 904-0495
[66]Osaka City University, Osaka 558-8585
[67]Research Center for Nuclear Physics, Osaka University, Osaka 567-0047
[68]Pacific Northwest National Laboratory, Richland, Washington 99352
[69]Panjab University, Chandigarh 160014
[70]Peking University, Beijing 100871
[71]Punjab Agricultural University, Ludhiana 141004
[72]Theoretical Research Division, Nishina Center, RIKEN, Saitama 351-0198
[73]Seoul National University, Seoul 08826
[74]Showa Pharmaceutical University, Tokyo 194-8543
[75]Soongsil University, Seoul 06978
[76]J. Stefan Institute, 1000 Ljubljana
[77]Taras Shevchenko National Univ. of Kiev, Kiev
[78]Tata Institute of Fundamental Research, Mumbai 400005
[79]Department of Physics, Technische Universität München, 85748 Garching
[80]Tel Aviv University, School of Physics and Astronomy, Tel Aviv, 69978
[81]Department of Physics, Tohoku University, Sendai 980-8578
[82]Tokyo Institute of Technology, Tokyo 152-8550
[83]Tokyo Metropolitan University, Tokyo 192-0397
[84]Universidad Autonoma de Sinaloa, Sinaloa 80000
[85]Dipartimento di Scienze Fisiche, Università di Napoli Federico II, I-80126 Napoli
[86]Dipartimento di Fisica e Astronomia, Università di Padova, I-35131 Padova
[87]Dipartimento di Fisica, Università di Perugia, I-06123 Perugia
[88]Dipartimento di Fisica, Università di Pisa, I-56127 Pisa
[89]Dipartimento di Matematica e Fisica, Università di Roma Tre, I-00146 Roma
[90]Dipartimento di Fisica, Università di Torino, I-10125 Torino
[91]Dipartimento di Fisica, Università di Trieste, I-34127 Trieste
[92]Université de Montréal, Physique des Particules, Montréal, Québec, H3C 3J7
[93]Université de Strasbourg, CNRS, IPHC, UMR 7178, 67037 Strasbourg
[94]University of Bonn, 53115 Bonn
[95]University of British Columbia, Vancouver, British Columbia, V6T 1Z1
[96]University of Cincinnati, Cincinnati, Ohio 45221
[97]University of Hawaii, Honolulu, Hawaii 96822
[98]Faculty of Mathematics and Physics, University of Ljubljana, 1000 Ljubljana
[99]University of Louisville, Louisville, Kentucky 40292
[100]National Centre for Particle Physics, University Malaya, 50603 Kuala Lumpur
[101]University of Maribor, 2000 Maribor
[102]School of Physics, University of Melbourne, Victoria 3010
[103]University of Mississippi, University, Mississippi 38677
[104]University of Miyazaki, Miyazaki 889-2192
[105]University of Pittsburgh, Pittsburgh, Pennsylvania 15260
[106]University of Science and Technology of China, Hefei 230026
[107]University of South Alabama, Mobile, Alabama 36688
[108]University of South Carolina, Columbia, South Carolina 29208
[109]School of Physics, University of Sydney, New South Wales 2006
[110]Department of Physics, University of Tokyo, Tokyo 113-0033
[111]Kavli Institute for the Physics and Mathematics of the Universe (WPI), University of Tokyo, Kashiwa 277-8583
[112]University of Victoria, Victoria, British Columbia, V8W 3P6
[113]Virginia Polytechnic Institute and State University, Blacksburg, Virginia 24061
[114]Wayne State University, Detroit, Michigan 48202
[115]Yamagata University, Yamagata 990-8560
[116]Alikhanyan National Science Laboratory, Yerevan 0036
[117]Yonsei University, Seoul 03722

Theories beyond the standard model often predict the existence of an additional neutral boson, the Z'. Using data collected by the Belle II experiment during 2018 at the SuperKEKB collider, we perform the first searches for the invisible decay of a Z' in the process $e^+e^- \to \mu^+\mu^- Z'$ and of a lepton-flavor-violating Z' in $e^+e^- \to e^\pm\mu^\mp Z'$. We do not find any excess of events and set 90% credibility level upper limits on the cross sections of these processes. We translate the former, in

the framework of an $L_\mu - L_\tau$ theory, into upper limits on the Z' coupling constant at the level of $5 \times 10^{-2} \div 1$ for $M_{Z'} \leq 6\,\mathrm{GeV}/c^2$.

PACS numbers: 12.60.-i, 14.80.-j, 13.66.De, 95.35.+d

The standard model (SM) is a successful and highly predictive theory of fundamental particles and interactions. However, it cannot be considered a complete description of nature, as it does not account for many phenomena, including dark matter.

The $L_\mu - L_\tau$ extension of the SM [1, 2] gauges the difference of the leptonic muon and tau number, giving rise to a new vector boson, the Z'. The Z' couples to the SM only through the μ, τ, ν_μ and ν_τ, with coupling constant g'. The $L_\mu - L_\tau$ model is potentially able to address important open issues in particle physics, including the anomalies in the $b \to s\mu^+\mu^-$ decays reported by the LHCb experiment [3], the anomaly in the muon anomalous magnetic moment $(g-2)_\mu$ [4], and dark matter phenomenology, if extra matter is charged under $L_\mu - L_\tau$ [1, 5]. We investigate here, for the first time, the specific invisible decay topology $e^+e^- \to \mu^+\mu^- Z'$, $Z' \to$ invisible, where the Z' production occurs via radiation off a final state muon. The decay branching fractions (BF) to neutrinos are predicted to vary between 33% and 100% depending on the Z' mass [5]. This model ("standard Z'" in the following) is poorly constrained at low masses. Related searches have been performed by the *BABAR* and CMS experiments for a Z' decaying to muons [6, 7]. Our search is, therefore, the first to have sensitivity to Z' masses $m_{Z'} < 2m_\mu$. If the Z' is able to decay directly into a pair of dark matter particles $\chi\bar{\chi}$, one expects $\mathrm{BF}(Z' \to \chi\bar{\chi}) \approx 1$. We provide separate results for this scenario, which is not constrained by existing measurements.

The second scenario we consider postulates the existence of a lepton-flavor-violating (LFV) boson, either a scalar or a vector ("LFV Z'" in the following), which couples to leptons [8, 9]. We focus on the LFV $e - \mu$ coupling. While the presence of LFV mediators can be constrained by measurements of the forward-backward asymmetry in $e^+e^- \to \mu^+\mu^-$ [9, 10], we present here a direct, model-independent search of $e^+e^- \to e^\pm\mu^\mp Z'$, $Z' \to$ invisible. The presence of missing energy decays make these searches especially suitable for an e^+e^- collider.

The Belle II detector [11] operates at the SuperKEKB electron-positron collider [12], located at the KEK laboratory in Tsukuba, Japan. Data were collected at the center-of-mass (CM) energy of the $\Upsilon(4S)$ resonance from April to July 2018. The energies of the electron and positron beams are 7 GeV and 4 GeV, respectively, resulting in a boost of $\beta\gamma = 0.28$ of the CM frame relative to the lab frame. The integrated luminosity used in this analysis amounts to $276\,\mathrm{pb}^{-1}$ [13].

The Belle II detector consists of several subdetectors arranged around the beam pipe in a cylindrical structure. A superconducting solenoid, situated outside of the calorimeter, provides a 1.5 T magnetic field. Subdetectors relevant for this analysis are briefly described here; a description of the full detector is given in [11, 14]. The innermost subdetector is the vertex detector (VXD), which includes two layers of silicon pixels and four outer layers of silicon strips. Only a single octant of the VXD was installed during the 2018 operations [15]. The main tracking device (CDC) is a large helium-based small-cell drift chamber. The electromagnetic calorimeter (ECL) consists of a barrel and two endcaps made of CsI(Tl) crystals. The z axis of the laboratory frame is along the detector solenoidal axis in the direction of the electron beam. "Longitudinal" and "transverse" are with respect to this direction, unless otherwise specified.

The invisible Z' signature is a peak in the distribution of the invariant mass of the system recoiling against a lepton pair. "Recoil" quantities such as mass and momentum refer to this system. They coincide with Z' properties in the case of signal events and typically correspond to undetected SM particles in the case of background events. The analysis uses events with exactly two tracks, identified as $\mu\mu$ or $e\mu$, and minimal other activity in the ECL. The standard Z' selection is optimized using simulated events prior to examining data; the same criteria, aside from an electron in the final state, are used for the LFV Z' search. The dominant backgrounds are SM final states with missing energy and two tracks identified as leptons. These are radiative muon pairs ($e^+e^- \to \mu^+\mu^-\gamma(\gamma)$) with one or more photons which are not detected due to inefficiency or acceptance, $e^+e^- \to \tau^+\tau^-(\gamma)$, and $e^+e^- \to e^+e^-\mu^+\mu^-$ with electrons outside the acceptance. Control samples are used to check background rates predicted by simulation and to infer correction factors and related uncertainties. Upper limits on the standard Z' cross section are computed with a counting technique in windows of the recoil mass distribution. For the LFV Z' model-independent search, upper limits are interpreted in terms of signal efficiency times cross section. Details of each of these steps are described below.

Signal events are generated with `MadGraph 5` [16] for standard Z' masses ranging from 0.5 to $8\,\mathrm{GeV}/c^2$ in steps of $0.5\,\mathrm{GeV}/c^2$. The following background sources are generated using the specified generators: $e^+e^- \to \mu^+\mu^-(\gamma)$ (`KKMC` [17]); $e^+e^- \to \pi^+\pi^-(\gamma)$ (`PHOKHARA` [18]); $e^+e^- \to e^+e^-(\gamma)$ (`BabaYaga@NLO` [19]); $e^+e^- \to \tau^+\tau^-(\gamma)$ (`KKMC` [17] with `TAUOLA` [20]); $e^+e^- \to e^+e^-\mu^+\mu^-$; and $e^+e^- \to e^+e^-e^+e^-$ (`AAFH` [21]). The detector geometry and the interactions of the final

state particles with the material are simulated using `Geant4` [22] and the Belle II Analysis Software Framework [23].

The standard Z' search uses the CDC two-track trigger, which selects events with at least two tracks with an azimuthal opening angle larger than 90°. The LFV Z' search uses the ECL trigger, which selects events with total energy in the barrel and part of the endcap above 1 GeV. Both triggers reject events that are consistent with being Bhabha scatterings.

To reject spurious tracks and beam induced background, "good" tracks are required to have transverse and longitudinal projections of the distance of closest approach with respect to the interaction point smaller than 0.5 cm and 2.0 cm, respectively. Photons are classified as ECL clusters with energy greater than 100 MeV, which are not associated with tracks. Quantities are defined in the laboratory frame unless specified otherwise. Events are required to pass the following selection criteria.

1. Exactly two oppositely charged good tracks, with polar angles in a restricted barrel ECL acceptance $\theta \in [37, 120]^\circ$ and with azimuthal opening angle $> 90^\circ$, to match the CDC trigger requirement.

2. Recoil momentum pointing into the ECL barrel acceptance $\theta \in [32, 125]^\circ$, to exclude inefficient regions where photons from radiative backgrounds can pass undetected. This selection is applied only for recoil masses below $3\,\mathrm{GeV}/c^2$; missed radiative photons are unlikely to produce higher masses.

3. An ECL-based particle identification (PID) selection: $0.15 < E < 0.4\,\mathrm{GeV}$ and $E/pc < 0.4$ for muons; $0.8 < E/pc < 1.2$ and $E > 1.5\,\mathrm{GeV}$ for electrons, where E is the energy of the ECL cluster associated to a track of momentum p.

4. No photons within a 15° cone around the recoil momentum direction in the CM frame, to suppress radiative lepton pair backgrounds.

5. Total photon energy less than 0.4 GeV and no π^0 candidates (pairs of photons with invariant masses within $10\,\mathrm{MeV}/c^2$ of the nominal π^0 value)

After this selection, the background for recoil masses below $7\,\mathrm{GeV}/c^2$ is dominated by $e^+e^- \to \tau^+\tau^-(\gamma)$ events with $\tau \to \mu$, or $\tau \to \pi$ where the pion is misidentified as a muon.

In subsequent steps of the analysis, events are grouped into windows of recoil mass. The width of these windows is $\pm 2\sigma$, where σ is the recoil mass resolution. It is obtained by fitting each Z' recoil mass distribution with a sum of a Crystal Ball (CB) [24–26] and a Gaussian function with coincident peaks. The resolution is computed as the sum in quadrature of the CB and Gaussian widths weighted according to their contributions. The choice of $\pm 2\sigma$ maximizes a figure of merit (FOM) [27] over the full spectrum. Mass window widths vary from $1150\,\mathrm{MeV}/c^2$ at $M_{Z'} = 0.5\,\mathrm{GeV}/c^2$ to a minimum of $51\,\mathrm{MeV}/c^2$ at $M_{Z'} = 6.9\,\mathrm{GeV}/c^2$. There are in total 69 mass windows below $8\,\mathrm{GeV}/c^2$.

A final selection, denoted as "τ suppression", exploits the kinematics of the Z' production, which occurs radiatively from a final state muon, to further suppress $\tau^+\tau^-$ events in which the missing momentum arises from neutrinos from both τ decays. The variables, defined in the CM frame, are: the transverse recoil momentum with respect to the lepton with the higher momentum $p_{\mathrm{rec}}^{\mathrm{T,lmax}}$; with respect to the lower momentum $p_{\mathrm{rec}}^{\mathrm{T,lmin}}$; the transverse momentum of the dilepton pair ($p_{\mu\mu}^{\mathrm{T}}$ or $p_{e\mu}^{\mathrm{T}}$). Figure 1 shows $p_{\mathrm{rec}}^{\mathrm{T,lmax}}$ versus $p_{\mathrm{rec}}^{\mathrm{T,lmin}}$ for a standard Z' mass of $3\,\mathrm{GeV}/c^2$ and for the total simulated background in the corresponding recoil mass window.

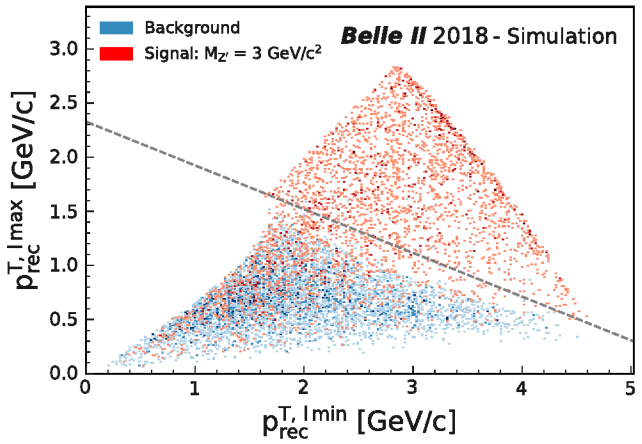

Fig. 1: $p_{\mathrm{rec}}^{\mathrm{T,lmax}}$ vs. $p_{\mathrm{rec}}^{\mathrm{T,lmin}}$ distributions after the optimal $p_{\mu\mu}^{\mathrm{T}}$ selection for $M_{Z'} = 3\,\mathrm{GeV}/c^2$ signal (red) and for background (blue). $p_{\mathrm{rec}}^{\mathrm{T,lmax}}$ ($p_{\mathrm{rec}}^{\mathrm{T,lmin}}$) is the transverse recoil momentum with respect to the direction of the muon with maxiumum (minimum) momentum in the CM frame. The optimal separation line is superimposed.

For the standard Z' search, a linear cut is imposed in the $p_{\mathrm{rec}}^{\mathrm{T,lmax}}$–$p_{\mathrm{rec}}^{\mathrm{T,lmin}}$ plane and a selection $p_{\mu\mu}^{\mathrm{T}} > p_{\mathrm{cut}}^{\mathrm{T}}$ where the cut values are determined using an optimization procedure that numerically maximizes the FOM in each recoil mass window. $p_{\mathrm{cut}}^{\mathrm{T}}$ is typically $1.5 \div 2.0\,\mathrm{GeV}/c$ and is effective in suppressing the remaining $\mu^+\mu^-(\gamma)$ and $e^+e^-\mu^+\mu^-$ backgrounds. For masses higher than $7\,\mathrm{GeV}/c^2$, signal and background overlap in the $p_{\mathrm{rec}}^{\mathrm{T,lmax}}$–$p_{\mathrm{rec}}^{\mathrm{T,lmin}}$ plane and effective separation lines are not found. The same values are used for the LFV Z' search.

Trigger, tracking and particle identification efficiencies are studied on control samples. The performance of the CDC two-track trigger is studied on data samples, mostly radiative Bhabha scattering events, selected by means of the ECL trigger. The efficiency is $(79 \pm 5)\%$ when both tracks are within the acceptance of selection 1; the un-

certainty is systematic and is due to kinematic dependencies. The performance of the ECL trigger is studied using $e^+e^- \to \mu^+\mu^-\gamma$ events with $E_\gamma > 1\,\text{GeV}$ that are selected with the CDC two-track trigger. The efficiency is found to be uniformly $(96 \pm 1)\%$ in the ECL barrel region.

The tracking efficiency for data is compared to simulation using radiative Bhabha and $e^+e^- \to \tau^+\tau^-$ events. Differences are found to be 10% for two-track final states, with a 4% systematic uncertainty due to kinematic dependencies.

The PID efficiency for data is compared to simulation using samples of four-lepton events from two-photon mediated processes. Discrepancies at the level of 2% per track are found, resulting in a systematic uncertainty of 4%.

The dimuon recoil mass resolution of data is compared to simulation using $e^+e^- \to \mu^+\mu^-\gamma$ events that are consistent with the full event energy, and which satisfy selections 1-5 except selection 4, which they are required to fail ($\mu\mu\gamma$ sample). The two-dimensional muon momentum distributions are reweighted to produce analogous distributions for $e^+e^- \to \mu^+\mu^- Z'$ events with Z' masses up to $3\,\text{GeV}/c^2$. The recoil mass widths for data and simulation are consistent, and no systematic uncertainty is assigned.

The selection criteria before the τ suppression are studied using signal-free control samples in data and simulation. The $\mu\mu\gamma$ sample is useful for the low recoil mass region. Similar $ee\gamma$ and $e\mu\gamma$ control samples are used for consistency checks. We also select $\mu\mu$ and $e\mu$ samples that satisfy requirements 1–5, but which fail the $p_{\text{rec}}^{\text{T,lmax}}$–$p_{\text{rec}}^{\text{T,lmin}}$ requirement. These studies indicate that the efficiency before the τ suppression is 35% lower for $\mu^+\mu^-$ events in data than in simulation, and 10% lower for $e^\pm\mu^\mp$ events. The latter is explained by tracking inefficiency, leaving a -25% unexplained deficit in dimuon events. A variety of studies failed to uncover the source of this discrepancy, which is consistently found to be independent of all checked quantities, including the recoil mass. The background predictions from simulation and the signal efficiency are thus corrected with scaling factors of 0.65 for $\mu^+\mu^-$ events and 0.9 for $e^\pm\mu^\mp$ events. The background level before the τ suppression selection is measured with a 2% statistical uncertainty in both samples [28], which is used as a systematic uncertainty. This is a strong constraint for the standard Z' signal efficiency as well, as the topology of background and signal events (a pair of muons and missing energy) is identical for signal and background and the discrepancy in the measured yield is found not to depend on kinematic quantities (see above). We nevertheless conservatively assign a systematic uncertainty of 12.5% on the correction factor to the signal efficiency for the dimuon sample, half the size of the observed discrepancy.

To study the τ suppression, we use an e^+e^- sample selected using the same analysis criteria, but with both tracks satisfying the electron criteria in selection 3. The resulting sample includes $e^+e^-\gamma$, $e^+e^-e^+e^-$ and $\tau^+\tau^-$ events where both leptons decay to electrons. The latter has the same kinematic features of the most relevant background source to both searches. Agreement between data and simulation is found after the τ suppression, within a 22% statistical uncertainty. This is taken as a systematic uncertainty on the background; no systematic uncertainty due to this effect is considered for the signal, as the selection has a high efficiency (around 50%, slightly depending on the Z' mass), and the distributions on which it is based are well reproduced in simulation.

After the corrections for the two-track trigger efficiency and for the data/simulation discrepancy in $\mu^+\mu^-$ events, signal efficiencies are found to range between 2.6% and 4.9% for Z' masses below $7\,\text{GeV}/c^2$. Signal efficiencies are interpolated from the generated Z' masses to the center of each recoil mass window. An additional binning scheme is introduced with a shift of a half bin, to cover hypothetical signals located at the border of two contiguous bins, where the signal efficiency is reduced. Systematic uncertainties are summarized in Table I.

Table I: Relative systematic uncertainties affecting the $\mu^+\mu^-$ and $e^\pm\mu^\mp$ analyses.

Source	$\mu^+\mu^-$	$e^\pm\mu^\mp$
Trigger efficiency	6%	1%
Tracking efficiency	4%	4%
PID	4%	4%
Luminosity	0.7%	0.7%
τ suppression (background)	22%	22%
Background before τ suppression	2%	2%
Discrepancy in $\mu\mu$ yield (signal)	12.5%	-

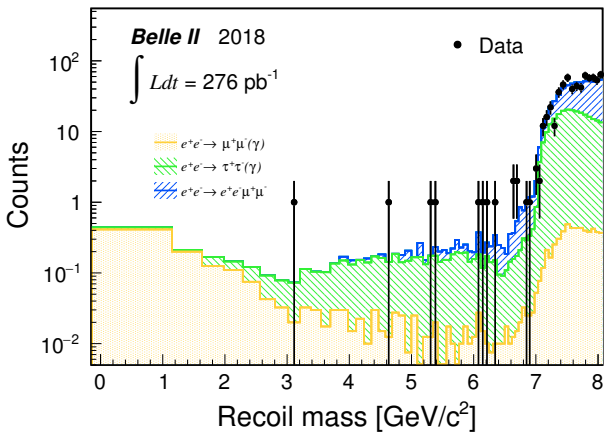

Fig. 2: Recoil mass spectrum of the $\mu^+\mu^-$ sample. Simulated samples (histograms) are rescaled for luminosity, trigger efficiency (0.79) and correction factor (0.65, see text). Histogram bin widths indicate the recoil mass windows.

The final recoil mass spectrum of the $\mu^+\mu^-$ sample is shown in Fig. 2, together with background simulations. We look for the presence of possible local excesses by calculating for each recoil mass window the probability to obtain a yield greater or equal to that obtained in data given the predicted background, including statistical and systematic uncertainties. No anomalies are observed, with all results below 3σ local significance in both the normal and shifted-binning options [28]. A Bayesian procedure [29] is used to compute 90% credibility level (CL) upper limits on the standard Z' cross section. We assume flat priors for all positive values of the cross section, while Poissonian likelihoods are assumed for the number of observed and simulated events. Gaussian smearing is used to model the systematic uncertainties. Results are cross-checked with log-flat priors and with a frequentist procedure based on the Feldman-Cousins approach [30] and are found to be compatible in both cases [28]. Cross section results are translated into 90% CL upper limits on the coupling constant g'. These are shown in Fig. 3, where only values $g' \leq 1$ are displayed.

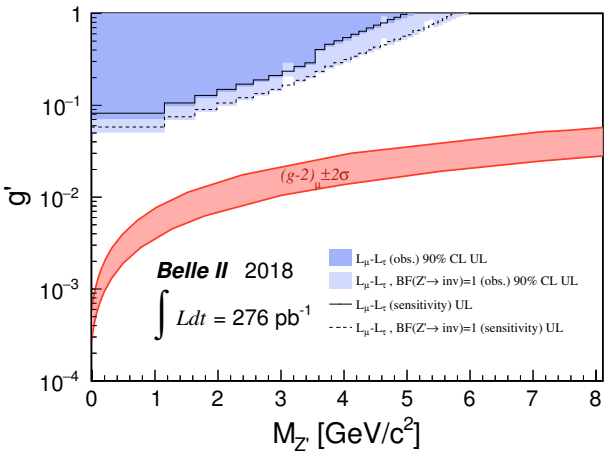

Fig. 3: 90% CL upper limits on coupling constant g'. Dark blue filled areas show the exclusion regions for g' at 90% CL, assuming the $L_\mu - L_\tau$ predicted BF for $Z' \to$ invisible; light blue areas are for BF($Z' \to$ invisible) $= 1$. The solid and dashed lines are the expected sensitivities in the two hypotheses. The red band shows the region that could explain the muon anomalous magnetic moment $(g-2)_\mu \pm 2\sigma$ [1, 5].

The final recoil mass spectrum of the $e^\pm\mu^\mp$ sample is shown in Fig. 4, together with background simulations. Again, no anomalies are observed above 3σ local significance [28]. Model-independent 90% CL upper limits on the LFV Z' efficiency times cross section are computed using the Bayesian procedure described above and cross-checked with a frequentist Feldman-Cousins procedure (Fig. 5). Additional plots and numerical results can be found in the supplemental material [28].

In summary, we have searched for an invisibly decaying Z' boson in the process $e^+e^- \to \mu^+\mu^- Z'$ and for a

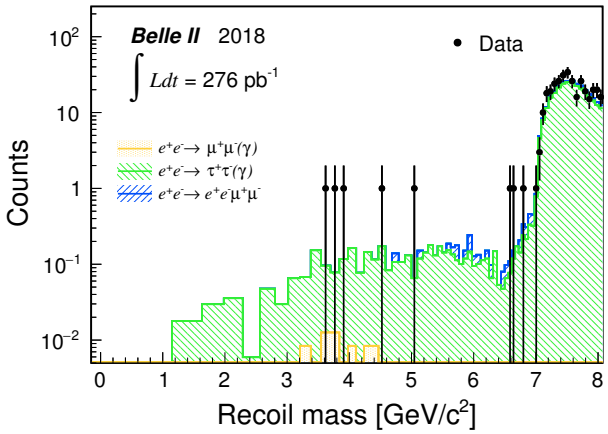

Fig. 4: Recoil mass spectrum of the $e^\pm\mu^\mp$ sample. Simulated samples (histograms) are rescaled for luminosity, trigger efficiency (0.96) and correction factor (0.9, see text). Histogram bin widths indicate the recoil mass windows.

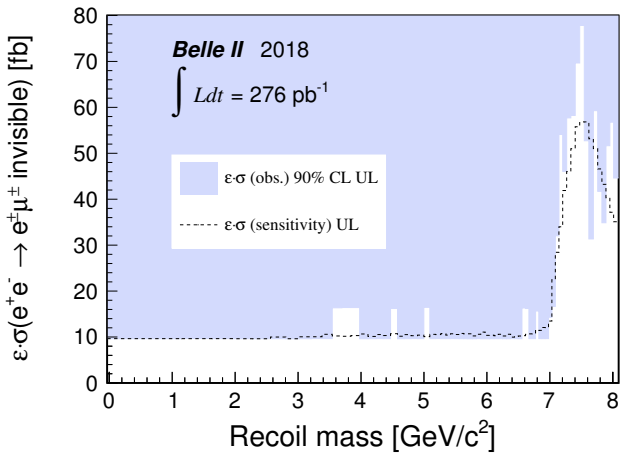

Fig. 5: 90% CL upper limits on efficiency times cross section $\epsilon \times \sigma[e^+e^- \to e^\pm\mu^\mp \text{invisible}]$. The dashed line is the expected sensitivity.

LFV Z' in the process $e^+e^- \to e^\pm\mu^\mp Z'$, using 276 pb^{-1} of data collected by Belle II at SuperKEKB in 2018. We find no significant excess and set for the first time 90% CL upper limits on the coupling constant g' in the range 5×10^{-2} to 1 for the former case and to the efficiency times cross section around 10 fb for the latter. The full Belle II data set, with better muon identification, a deeper knowledge of the detector, and the use of multivariate analysis techniques should enable the full $(g-2)_\mu$ band to be probed in the future.

We thank the SuperKEKB group for the excellent operation of the accelerator; the KEK cryogenics group for the efficient operation of the solenoid; and the KEK computer group for on-site computing support. This work was supported by the following funding sources: Science Committee of the Republic of Armenia Grant No. 18T-

1C180; Australian Research Council and research grant Nos. DP180102629, DP170102389, DP170102204, DP150103061, FT130100303, and FT130100018; Austrian Federal Ministry of Education, Science and Research, and Austrian Science Fund No. P 31361-N36; Natural Sciences and Engineering Research Council of Canada, Compute Canada and CANARIE; Chinese Academy of Sciences and research grant No. QYZDJ-SSW-SLH011, National Natural Science Foundation of China and research grant Nos. 11521505, 11575017, 11675166, 11761141009, 11705209, and 11975076, LiaoNing Revitalization Talents Program under contract No. XLYC1807135, Shanghai Municipal Science and Technology Committee under contract No. 19ZR1403000, Shanghai Pujiang Program under Grant No. 18PJ1401000, and the CAS Center for Excellence in Particle Physics (CCEPP); the Ministry of Education, Youth and Sports of the Czech Republic under Contract No. LTT17020 and Charles University grants SVV 260448 and GAUK 404316; European Research Council, 7th Framework PIEF-GA-2013-622527, Horizon 2020 Marie Sklodowska-Curie grant agreement No. 700525 'NIOBE,' Horizon 2020 Marie Sklodowska-Curie RISE project JENNIFER grant agreement No. 644294, Horizon 2020 ERC-Advanced Grant No. 267104, and NewAve No. 638528 (European grants); L'Institut National de Physique Nucléaire et de Physique des Particules (IN2P3) du CNRS (France); BMBF, DFG, HGF, MPG and AvH Foundation (Germany); Department of Atomic Energy and Department of Science and Technology (India); Israel Science Foundation grant No. 2476/17 and United States-Israel Binational Science Foundation grant No. 2016113; Istituto Nazionale di Fisica Nucleare and the research grants BELLE2; Japan Society for the Promotion of Science, Grant-in-Aid for Scientific Research grant Nos. 16H03968, 16H03993, 16H06492, 16K05323, 17H01133, 17H05405, 18K03621, 18H03710, 18H05226, 19H00682, 26220706, and 26400255, the National Institute of Informatics, and Science Information NETwork 5 (SINET5), and the Ministry of Education, Culture, Sports, Science, and Technology (MEXT) of Japan; National Research Foundation (NRF) of Korea Grant Nos. 2016R1D1A1B01010135, 2016R1D1A1B02012900, 2018R1A2B3003643, 2018R1A6A1A06024970, 2018R1D1A1B07047294, 2019K1A3A7A09033840, and 2019R1-I1A3A01058933, Radiation Science Research Institute, Foreign Large-size Research Facility Application Supporting project, the Global Science Experimental Data Hub Center of the Korea Institute of Science and Technology Information and KREONET/GLORIAD; Universiti Malaya RU grant, Akademi Sains Malaysia and Ministry of Education Malaysia; Frontiers of Science Program contracts FOINS-296, CB-221329, CB-236394, CB-254409, and CB-180023, and the Thematic Networks program (Mexico); the Polish Ministry of Science and Higher Education and the National Science Center; the Ministry of Science and Higher Education of the Russian Federation, Agreement 14.W03.31.0026; Slovenian Research Agency and research grant Nos. J1-9124 and P1-0135; Agencia Estatal de Investigacion, Spain grant Nos. FPA2014-55613-P and FPA2017-84445-P, and CIDEGENT/2018/020 of Generalitat Valenciana; Ministry of Science and Technology and research grant Nos. MOST106-2112-M-002-005-MY3 and MOST107-2119-M-002-035-MY3, and the Ministry of Education (Taiwan); Thailand Center of Excellence in Physics; TUBITAK ULAKBIM (Turkey); Ministry of Education and Science of Ukraine; the US National Science Foundation and research grant Nos. PHY-1807007 and PHY-1913789, and the US Department of Energy and research grant Nos. DE-AC06-76RLO1830, DE-SC0007983, DE-SC0009824, DE-SC0009973, DE-SC0010073, DE-SC0010118, DE-SC0010504, DE-SC0011784, DE-SC0012704; and the National Foundation for Science and Technology Development (NAFOSTED) of Vietnam under contract No 103.99-2018.45.

[1] B. Shuve and I. Yavin, Phys. Rev. D **89**, 113004 (2014).
[2] W. Altmannshofer, S. Gori, S. Profumo, and F. S. Queiroz, JHEP **12**, 106 (2016).
[3] R. Aaij *et al.* (LHCb Collaboration), Phys. Rev. Lett. **113**, 151601 (2014).
[4] G. W. Bennett *et al.* (Muon g-2 Collaboration), Phys. Rev. D **73**, 072003 (2006).
[5] D. Curtin, R. Essig, S. Gori, and J. Shelton, JHEP **02**, 157 (2015).
[6] J. P. Lees *et al.* (*BABAR* Collaboration), Phys. Rev. D **94**, 011102 (2016).
[7] A. M. Sirunyan *et al.* (CMS Collaboration), Phys. Lett. **B792**, 345 (2019).
[8] I. Galon and J. Zupan, JHEP **05**, 083 (2017).
[9] I. Galon, A. Kwa, and P. Tanedo, JHEP **03**, 064 (2017).
[10] J. Abdallah *et al.* (DELPHI Collaboration), Eur. Phys. J. **C45**, 589 (2006).
[11] T. Abe *et al.* (Belle II Collaboration), (2010), arXiv:1011.0352 [physics.ins-det] .
[12] K. Akai, K. Furukawa, and H. Koiso (SuperKEKB), Nucl. Instrum. Meth. **A907**, 188 (2018).
[13] F. Abudinén *et al.* (Belle II Collaboration), (2019), accepted for publication by Chin. Phys. C, arXiv:1910.05365 [hep-ex] .
[14] E. Kou, P. Urquijo, *et al.*, (2018), accepted for publication by PTEP, arXiv:1808.10567 [hep-ex] .
[15] A. Paladino, in *Proc. 62nd ICFA ABDW on High Luminosity Circular e^+e^- Colliders (eeFACT'18), Hong Kong, China, 24-27 September 2018*, ICFA ABDW on High Luminosity Circular e^+e^- Colliders No. 62 (2019) pp. 221–225.
[16] J. Alwall, R. Frederix, S. Frixione, V. Hirschi, F. Maltoni, O. Mattelaer, H. S. Shao, T. Stelzer, P. Torrielli, and M. Zaro, JHEP **07**, 079 (2014).

[17] S. Jadach, B. F. L. Ward, and Z. Was, Comput. Phys. Commun. **130**, 260 (2000).
[18] H. Czyż, M. Gunia, and J. H. Kühn, JHEP **08**, 110 (2013).
[19] G. Balossini, C. Bignamini, C. M. C. Calame, G. Montagna, O. Nicrosini, and F. Piccinini, Phys. Lett. **B663**, 209 (2008).
[20] N. Davidson, G. Nanava, T. Przedzinski, E. Richter-Was, and Z. Was, Comput. Phys. Commun. **183**, 821 (2012).
[21] F. A. Berends, P. H. Daverveldt, and R. Kleiss, Nucl. Phys. **B253**, 441 (1985).
[22] S. Agostinelli *et al.* (GEANT4), Nucl. Instrum. Meth. **A506**, 250 (2003).
[23] T. Kuhr, C. Pulvermacher, M. Ritter, T. Hauth, and N. Braun (Belle II Framework Software Group), Comput. Softw. Big Sci. **3**, 1 (2019).
[24] M. J. Oreglia, Ph.D. thesis, Stanford University (1980).
[25] J. E. Gaiser, Ph.D. thesis, Stanford University (1982).
[26] T. Skwarnicki, Ph.D. thesis, Cracow INP and DESY (1986).
[27] G. Punzi, *Statistical problems in particle physics, astrophysics and cosmology. Proceedings, Conference, PHYSTAT 2003, Stanford, USA, September 8-11, 2003*, eConf **C030908**, MODT002 (2003).
[28] See Supplemental Material at `http://XYZ` for additional plots.
[29] F. Beaujean, A. Caldwell, D. Greenwald, K. Kröninger, and O. Schulz, "Bat release, version 1.0.0," (2018).
[30] G. J. Feldman and R. D. Cousins, Phys. Rev. D **57**, 3873 (1998).

Search for an invisibly decaying Z' boson at Belle II in $e^+e^- \to \mu^+\mu^-(e^\pm\mu^\mp)$ plus missing energy final states

Belle II Collaboration

This material is submitted as supplementary information for the Electronic Physics Auxiliary Publication Service.

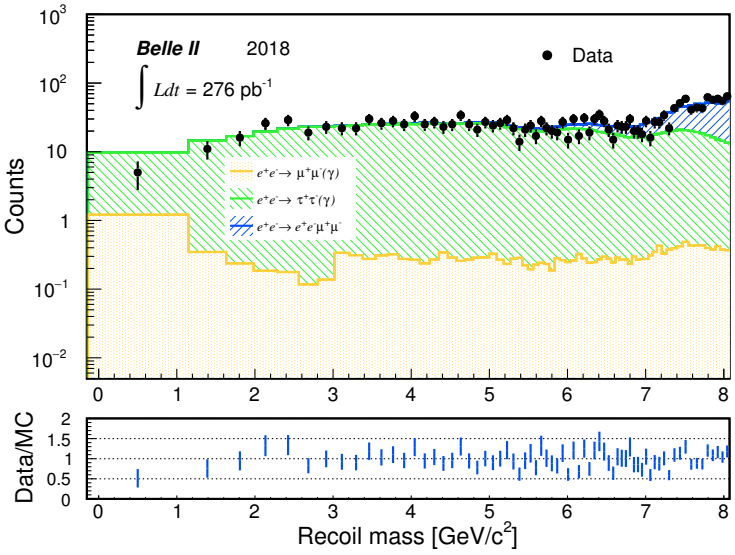

FIG. 1: Recoil mass spectrum for the $\mu^+\mu^-$ sample before the τ suppression selection. Simulated samples (histograms) are rescaled for luminosity, trigger efficiency (0.79) and correction factor (0.65, see text). Histogram bin widths indicate the recoil mass windows.

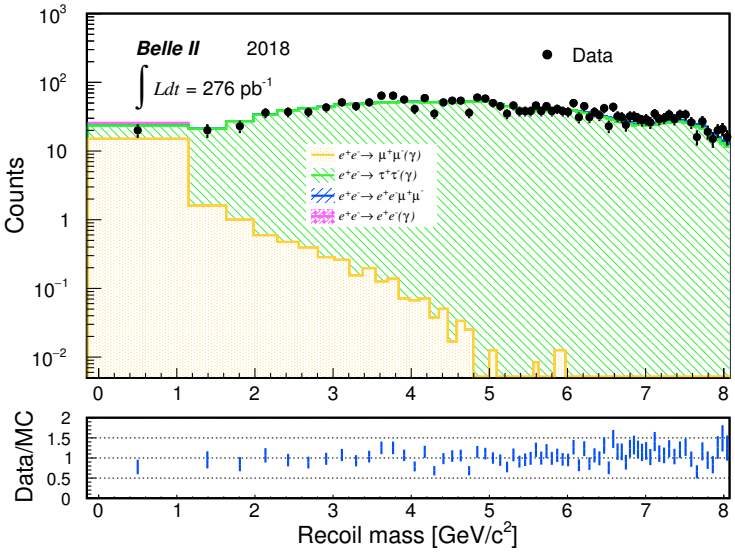

FIG. 2: Recoil mass spectrum for the $e^\pm\mu^\mp$ sample after the τ suppression selection. Simulated samples (histograms) are rescaled for luminosity, trigger efficiency (0.96) and correction factor (0.9, see text). Histogram bin widths indicate the recoil mass windows.

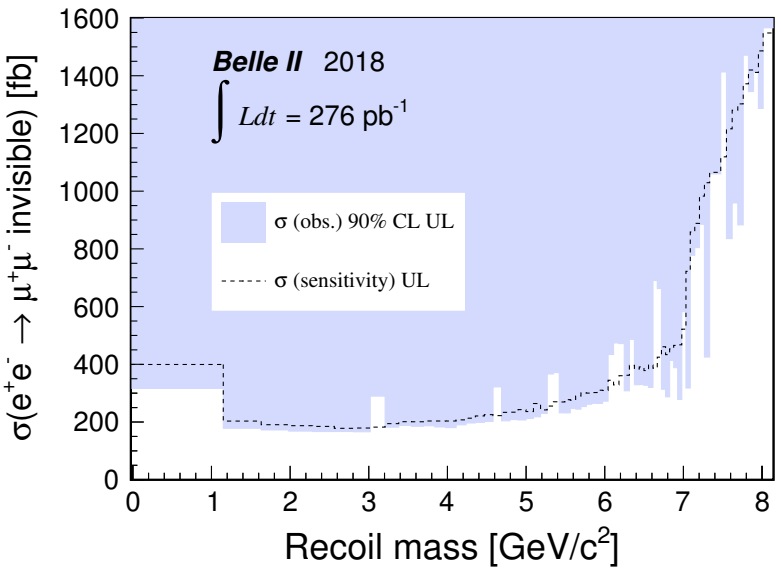

FIG. 3: 90% CL upper limits on cross section $\sigma(e^+e^- \to \mu^+\mu^-\text{invisible})$. The dashed line is the expected sensitivity.

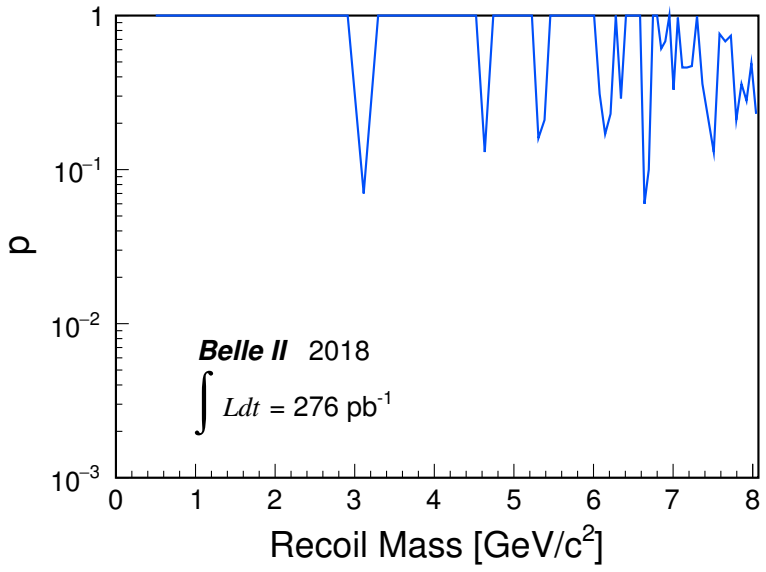

FIG. 4: Probability p to get a result greater or equal to the observed one given the predicted background level as a function of the recoil mass for the $\mu^+\mu^-$ sample.

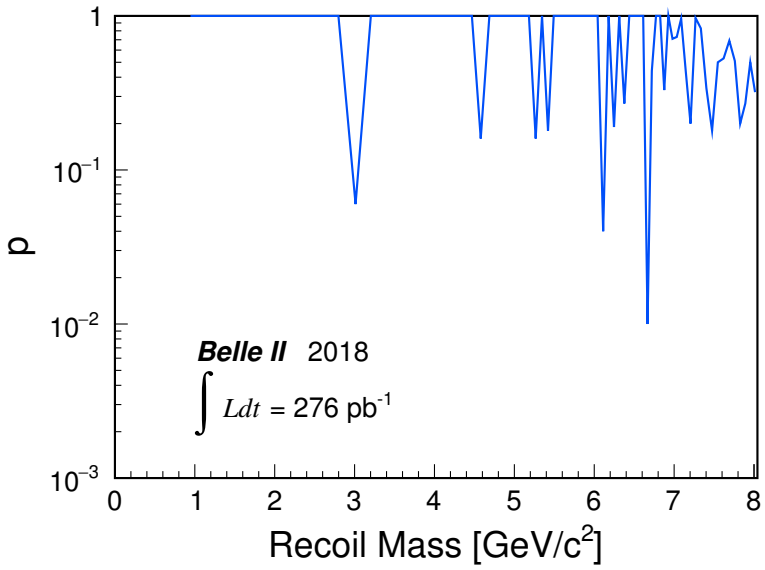

FIG. 5: Probability p to get a result greater or equal to the observed one given the predicted background level as a function of the recoil mass for the $\mu^+\mu^-$ sample, evaluated with a half bin shift.

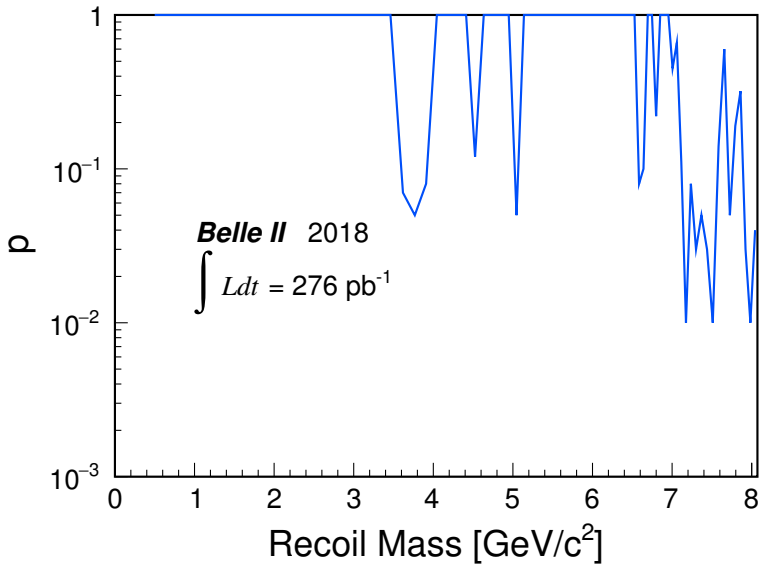

FIG. 6: Probability p to get a result greater or equal to the observed one given the predicted background level as a function of the recoil mass for the $e^{\pm}\mu^{\mp}$ sample.

TABLE I: Standard Z' mass windows, detected yields $N_{\rm obs}$, signal efficiency ϵ, expected number of background events $N_{\rm bkg}$, 90% CL upper limits on $\sigma(e^+e^- \to \mu^+\mu^-{\rm invisible})$, and 90% CL upper limits on g' (computed in the center of the Z' mass window).

Z' mass window [GeV/c^2]	$N_{\rm obs}$	ϵ	$N_{\rm bkg}$	σ [fb]	g'
-0.150-1.150	0	0.028	0.438	316	0.051
1.150-1.632	0	0.049	0.213	178	0.070
1.632-1.982	0	0.052	0.167	173	0.086
1.982-2.287	0	0.052	0.145	169	0.100
2.287-2.562	0	0.052	0.121	167	0.115
2.562-2.805	0	0.052	0.092	167	0.129
2.805-3.018	0	0.052	0.078	166	0.144
3.018-3.208	1	0.051	0.073	290	0.209
3.208-3.381	0	0.049	0.114	182	0.180
3.381-3.542	0	0.047	0.104	188	0.198
3.542-3.695	0	0.047	0.102	185	0.226
3.695-3.840	0	0.048	0.136	187	0.254
3.840-3.979	0	0.048	0.169	183	0.275
3.979-4.110	0	0.048	0.151	181	0.296
4.110-4.236	0	0.047	0.153	190	0.327
4.236-4.355	0	0.046	0.160	197	0.356
4.355-4.469	0	0.045	0.171	199	0.381
4.469-4.580	0	0.044	0.182	202	0.408
4.580-4.688	1	0.043	0.143	322	0.545
4.688-4.794	0	0.043	0.186	204	0.461
4.794-4.898	0	0.042	0.180	208	0.494
4.898-4.998	0	0.042	0.206	207	0.520
4.998-5.094	0	0.041	0.166	212	0.554
5.094-5.184	0	0.040	0.264	218	0.590
5.184-5.268	0	0.039	0.152	230	0.635
5.268-5.347	1	0.039	0.175	366	0.833
5.347-5.422	1	0.038	0.233	371	0.873
5.422-5.493	0	0.037	0.200	232	0.723
5.493-5.562	0	0.037	0.211	232	0.751
5.562-5.630	0	0.036	0.190	247	0.803
5.630-5.697	0	0.036	0.221	245	0.827
5.697-5.765	0	0.035	0.291	254	0.874
5.765-5.834	0	0.034	0.228	262	0.920
5.834-5.903	0	0.034	0.252	265	0.960
5.903-5.972	0	0.033	0.202	264	0.994
5.972-6.042	0	0.032	0.196	272	> 1
6.042-6.112	1	0.031	0.374	434	> 1
6.112-6.180	1	0.030	0.194	474	> 1
6.180-6.248	1	0.030	0.268	472	> 1
6.248-6.313	0	0.029	0.237	308	> 1
6.313-6.377	1	0.028	0.342	487	> 1
6.377-6.439	0	0.027	0.248	329	> 1
6.439-6.499	0	0.026	0.225	330	> 1
6.499-6.557	0	0.026	0.186	327	> 1
6.557-6.613	0	0.027	0.354	320	> 1
6.613-6.668	2	0.028	0.367	690	> 1
6.668-6.721	2	0.028	0.537	662	> 1
6.721-6.773	0	0.029	0.860	314	> 1
6.773-6.825	0	0.030	0.766	287	> 1
6.825-6.876	1	0.030	0.959	413	> 1
6.876-6.927	1	0.031	1.176	388	> 1
6.927-6.979	0	0.032	1.203	278	> 1
6.979-7.032	3	0.033	2.004	582	> 1
7.032-7.087	2	0.038	6.069	318	> 1
7.087-7.144	12	0.044	11.357	778	> 1
7.144-7.204	16	0.050	15.229	804	> 1
7.204-7.267	22	0.057	21.406	885	> 1

Continued on next page

TABLE I continued from previous page

Z' mass window [GeV/c^2]	$N_{\rm obs}$	ϵ	$N_{\rm bkg}$	σ [fb]	g'
7.267-7.334	12	0.064	26.799	425	> 1
7.334-7.403	36	0.071	32.765	1060	> 1
7.475-7.547	58	0.084	45.061	1413	> 1
7.547-7.620	40	0.082	47.553	836	> 1
7.620-7.691	44	0.081	49.545	959	> 1
7.691-7.761	42	0.079	49.448	883	> 1
7.761-7.827	62	0.077	51.369	1471	> 1
7.827-7.892	57	0.076	52.360	1345	> 1
7.892-7.953	58	0.074	50.480	1413	> 1
7.953-8.014	53	0.073	52.640	1287	> 1
8.014-8.072	64	0.071	54.018	1566	> 1

TABLE II: LFV Z' mass window, detected yields $N_{\rm obs}$, expected number of background events $N_{\rm bkg}$, 90% CL upper limits on efficiency times cross section $\epsilon \times \sigma(e^+e^- \to e^\pm\mu^\mp{\rm invisible})$.

Z' mass window [GeV/c^2]	$N_{\rm obs}$	$N_{\rm bkg}$	$\epsilon \times \sigma$ [fb]
-0.150-1.150	0	0.000-0.010	9.62
1.150-1.632	0	0.018	9.67
1.632-1.982	0	0.030	9.64
1.982-2.287	0	0.036	9.64
2.287-2.562	0	0.006	9.62
2.562-2.805	0	0.048	9.62
2.805-3.018	0	0.030	9.60
3.018-3.208	0	0.065	9.62
3.208-3.381	0	0.068	9.66
3.381-3.542	0	0.153	9.65
3.542-3.695	1	0.096	16.36
3.695-3.840	1	0.078	16.41
3.840-3.979	1	0.117	16.41
3.979-4.110	0	0.163	9.61
4.110-4.236	0	0.077	9.63
4.236-4.355	0	0.145	9.65
4.355-4.469	0	0.115	9.63
4.469-4.580	1	0.172	16.20
4.580-4.688	0	0.083	9.62
4.688-4.794	0	0.139	9.63
4.794-4.898	0	0.107	9.66
4.898-4.998	0	0.131	9.64
4.998-5.094	1	0.065	16.46
5.094-5.184	0	0.151	9.64
5.184-5.268	0	0.143	9.65
5.268-5.347	0	0.178	9.64
5.347-5.422	0	0.131	9.64
5.422-5.493	0	0.172	9.65
5.493-5.562	0	0.143	9.63
5.562-5.630	0	0.187	9.63
5.630-5.697	0	0.167	9.62
5.697-5.765	0	0.177	9.61
5.765-5.834	0	0.101	9.62
5.834-5.903	0	0.151	9.65
5.903-5.972	0	0.243	9.61
5.972-6.042	0	0.127	9.61
6.042-6.112	0	0.133	9.63
6.112-6.180	0	0.113	9.64
6.180-6.248	0	0.151	9.64
6.248-6.313	0	0.098	9.62
6.313-6.377	0	0.149	9.61
6.377-6.439	0	0.053	9.64
6.439-6.499	0	0.080	9.63
6.499-6.557	0	0.098	9.62
6.557-6.613	1	0.109	16.32
6.613-6.668	1	0.151	16.20
6.668-6.721	0	0.172	9.64
6.721-6.773	0	0.207	9.64
6.773-6.825	1	0.338	15.66
6.825-6.876	0	0.310	9.65
6.876-6.927	0	0.461	9.64
6.927-6.979	0	0.450	9.65
6.979-7.032	1	0.849	14.30
7.032-7.087	3	4.905	16.66
7.087-7.144	10	8.327	32.04
7.144-7.204	18	11.817	54.09
7.204-7.267	19	16.685	46.06
7.267-7.334	24	19.384	57.71

Continued on next page

TABLE II continued from previous page

Z' mass window [GeV/c^2]	$N_{\rm obs}$	$N_{\rm bkg}$	$\epsilon \times \sigma$ [fb]
7.334-7.403	26	22.504	58.24
7.403-7.475	31	25.539	69.66
7.475-7.547	34	26.179	77.82
7.547-7.620	26	26.301	52.73
7.620-7.691	16	23.941	31.35
7.691-7.761	26	22.620	59.28
7.761-7.827	19	19.767	41.71
7.827-7.892	15	17.611	34.88
7.892-7.953	20	15.609	51.65
7.953-8.014	20	13.736	56.78
8.014-8.072	16	12.557	44.62